

Preliminary CFD Parametric Simulations of Low- and Medium-Density Urban Layouts

Ritesh Wankhade – Free University of Bozen-Bolzano, Italy – riteshnarendra.wankhade@natec.unibz.it

Giovanni Pernigotto – Free University of Bozen-Bolzano, Italy – giovanni.pernigotto@unibz.it

Michele Larcher – Free University of Bozen-Bolzano, Italy – michele.larcher@unibz.it

Abstract

Most existing cities were not designed to exploit wind and air displacement phenomena to ensure pollutant dilution and enhance the effectiveness of natural ventilation of the built environment. Although this problem is well known in the literature, the majority of previous studies focused on real case studies or on parametric layouts often characterized by high-rise buildings, which are not typical for most Italian and European cities. In this framework, the goal of this research was to perform a preliminary CFD parametric study on street canyons with low- and medium-rise buildings, focusing on the different parameters impacting outdoor air displacement in an urban layout. Seven different configurations of street canyon were simulated with ANSYS Fluent, focusing on the air displacement around a low-, medium- or high-rise target building, located at the beginning, at the end, or in the middle of the street canyon, respectively. The velocity and pressure contour plots were analysed to understand the behavior of airflow around the buildings in the different configurations, discussing in such a way the natural ventilation potential.

1. Introduction

Advances in technology and facilities available in urban cities have caused rapid urbanization, leading to the transfer of the population from rural to urban areas in search of new opportunities. The United Nations estimates that, by the year 2030, 60 % of the population will live in urban areas with at least half a million inhabitants (United Nations, 2018). Compared to the current situation, this phenomenon will generate demand for the construction of new homes and buildings. As a result, concerns about urban environmental and human health issues, such as air quality, natural outdoor ventilation, and dilution of pollutants in the built

environment will grow (Li et al., 2020). If not properly managed, these urbanization trends will bring increased urban density, with limited spaces among buildings (e.g., parks, parking lots, trees, etc.). This will further reduce air flows coming from surrounding areas, affecting air quality and pollutant dilution (Li et al., 2020; Song et al., 2018).

For this reason, there are many studies that have been conducted on the phenomena of urban ventilation and effectiveness of natural ventilation in cities. In particular, several studies focused on the impact of different urban parameters on natural ventilation, working on generic layouts, real city layouts, or both. Guo et al. (2015) selected a typical urban area in Dalian, China, to perform a comparative and simulative analysis about air displacement due to wind using CFD tools. King et al. (2017) presented a relationship between incident angle and ventilation rate, using an isolated cube and an array of irregular cubes representing generic buildings. Peng et al. (2017) ran CFD simulations of ten identical buildings forming a street canyon to investigate wind-driven natural ventilation and pollutant diffusion at pedestrian level.

When working with building layouts, there are some aspects to consider, such as the space between buildings, the size of buildings, doors and windows, and the width of the streets adjacent to them. These parameters are useful for understanding the relationship between buildings, cities, and natural ventilation potential. Some of the important parameters are, for instance, building height, building density BD (Ding & Lam, 2019), floor area ratio FAR , building site coverage BSC , and street aspect ratio AR_{street} (Yang et al., 2020). Park et al. (2020) and Cheng et al. (2009) investigated the flow characteristics around step-up street canyons and ventilation performance with different aspect ratios using

Part of

Pernigotto, G., Patuzzi, F., Prada, A., Corrado, V., & Gasparella, A. (Eds.). 2023. Building simulation applications BSA 2022. bu.press.

<https://doi.org/10.13124/9788860461919>



CFD. Peng et al. (2019) used the floor area ratio and the building site coverage to find the correlation between urban morphological parameters and ventilation performance. By keeping the floor area ratio constant and changing the building site coverage, they established nine idealized building configurations to find the correlation between these urban morphological parameters and ventilation performance. Street canyons and their size can also influence natural ventilation performance. For example, Yang et al. (2020) and Chatzimichailidis et al. (2019) underlined the importance of the street canyon aspect ratio characterizing indoor and outdoor ventilation and flow patterns.

As observed in the literature, CFD simulations have been used to compare and discuss in more detail the results obtained from experiments. For instance, Padilla-Marcos et al. (2017) performed their simulation with Ansys Fluent for a generic building layout, with the aim of studying ways to increase natural ventilation potential in buildings. However, the majority of these studies, and, in particular, those which evaluate natural ventilation in street canyons, primarily focus on high-density or populated cities. As an example, Yuan and Ng (2012) examined the pedestrian-level natural ventilation performance in the context of a regular street grid in the high urban density of Mong Kok in Hong Kong.

Despite the variety of research, most of this has paid particular attention only to high-rise buildings, with limited investigation into low-density cities and low or medium-rise buildings, which are more representative and typical of several countries in the European Union, such as Italy. Therefore, the aim of this study was to perform a preliminary CFD parametric analysis for low or medium-rise buildings, focusing on the different parameters impacting outdoor air displacement in this kind of urban layout, and to discuss if there is a potential for natural ventilation of buildings, considering relative height and position in a street canyon.

2. Methodology

2.1 Generic Urban Buildings Layout

In this work, a generic street canyon layout was chosen. The shape of each building considered is cuboidal with a cross-section equal to 20 m x 20 m. Each floor of the building has a gross height of 4 m, assuming the internal room height of 2.8 m. The height of the high, medium, and low-rise target buildings are 36 m, 24 m, and 12 m, respectively. 10 buildings are positioned in a 5 x 2 rectangular array, where the target building, i.e., the object of the investigation, can be in the front corner, in the middle of the side, or in the rear corner. Different to other studies in the literature (Ding & Lam, 2019; Ramponi et al., 2015), the distances between adjacent buildings along the street canyon are modeled as significantly less than the street's width, i.e., 5 m distance against 20 m of street width. Figs. 1 to 4 show the different configurations of the building arrangements.

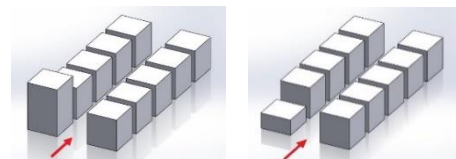


Fig. 1 – High-rise and low-rise building at corner (windward)

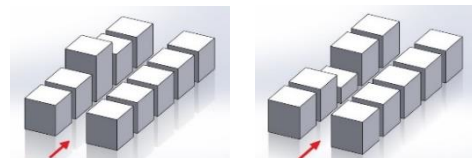


Fig. 2 – High-rise and low-rise building at side

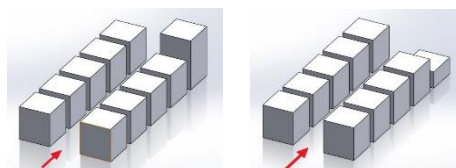


Fig. 3 – High-rise and low-rise building at corner (leeward)

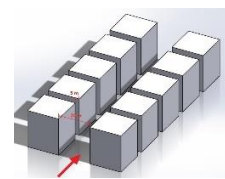


Fig. 4 – Buildings with same height

2.2 CFD Simulation

2.2.1 Computational Domain

The Ansys Fluent 19.0 simulation tool was used to simulate the cases mentioned in Section 2.1. The building geometries were drawn at full scale in Solidworks 2018 and then exported to Ansys Fluent. The computational domain size was based on previous examples from the literature, such as (Ding & Lam, 2019) and (Park et al., 2020). Following the examples of (Ding and Lam, 2019), the computational domain was set with a downstream length of eight times the building height (H) $8H$, an upstream length of $4H$, a lateral length of $4H$ on both sides of the buildings, and a height of $4H$. As a whole, the CFD domain size was set to 1560 m x 1020 m x 300 m (respectively, length, width, and height). The distance between the windward surface of the domain and the first building walls was equal to 450 m; both lateral distances between the surface of the domain and the walls of the building were 480 m; and the distance between the leeward surface of the domain and the wall surface of the rear building was equal to 930 m.

2.2.2 Meshing

Before setting up and running the CFD simulation, it was necessary to create a mesh. Following the literature (King et al., 2017), it was decided to use the hexahedral mesh for the entire domain in order to keep the resolution scheme simple. Fine meshing was applied on the buildings' walls in order to accurately capture the flow around them. The number of elements for the generic building layout cases ranged from 3 to 5.2 million.

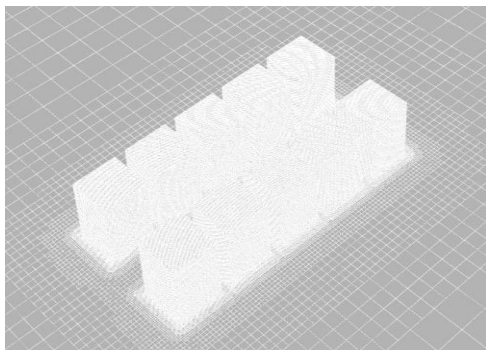


Fig. 5 – Mesh representation of generic building layout

2.2.3 Boundary Conditions and Numerical Setup

Choosing an appropriate boundary condition is an important step in CFD simulations. The windward surface of the domain was considered as the velocity inlet, and the lateral surfaces, the top surface, and the leeward surface of the domain as the pressure outlet. The velocity profile ($u(z)$) of inlet, the turbulent kinetic energy profile (k) and turbulent dissipation rate profile (ϵ) were calculated in agreement with the following equations (King et al., 2017):

$$u(z) = \frac{u^*}{\kappa} \ln \left(\frac{z+z_0}{z_0} \right) \quad (1)$$

$$k = \frac{u^{*2}}{\sqrt{C_\mu}} \quad (2)$$

and

$$\epsilon = \frac{u^{*3}}{\kappa(z+z_0)} \quad (3)$$

where u^* , z , z_0 are friction velocity (m/s), height coordinate (m), and roughness length (m), respectively. κ (≈ 0.41) and C_μ (≈ 0.09) are von Karman constant and a model constant, respectively. Referring to the meteorological data of Bolzano (typical year according to the Comitato Termotecnico Italiano), an average wind velocity of 1 m/s was chosen.

Reynolds-averaged Navier-Stokes (RANS) and Large Eddy Simulation (LES) are the most commonly used turbulence models for urban ventilation assessment. The accuracy of the LES turbulence model is higher than the RANS turbulence models, but it is also more expensive compared with the computational cost of the RANS turbulence models (Peng et al., 2019). RANS turbulence models are appropriate because of their simplicity, reasonable ventilation assessment results and less expensive computing power (Padilla-Marcos et al., 2017; Peng et al., 2019). The standard k - ϵ turbulence model was used. The standard k - ϵ model is a semi-empirical model based on model transport equations for the turbulence kinetic energy (k) and its dissipation rate (ϵ). The governing equations that were solved during the simulation in case standard k - ϵ turbulence model are the following:

$$\frac{\partial}{\partial t} (\rho k) + \frac{\partial}{\partial x_i} (\rho k u_i) = \frac{\partial}{\partial x_j} \left[\left(\mu + \frac{\mu_t}{\sigma_k} \right) \frac{\partial k}{\partial x_j} \right] + G_k - \rho \epsilon - Y_M \quad (4)$$

$$\frac{\partial}{\partial t} (\rho \epsilon) + \frac{\partial}{\partial x_i} (\rho \epsilon u_i) = \frac{\partial}{\partial x_j} \left[\left(\mu + \frac{\mu_t}{\sigma_\epsilon} \right) \frac{\partial \epsilon}{\partial x_j} \right] + C_{1\epsilon} \frac{\epsilon}{k} G_k - C_{2\epsilon} \rho \frac{\epsilon^2}{k} \quad (5)$$

$$\mu_t = \rho C_\mu \frac{k^2}{\epsilon} \quad (6)$$

In these equations, G_k represents the generation of turbulence kinetic energy due to the mean velocity gradients. Y_M represents the contribution of the fluctuating dilatation in compressible turbulence to the overall dissipation rate. $C_{1\varepsilon}$ (=1.44), $C_{2\varepsilon}$ (=1.92) and μ_t (=0.09) are constants. σ_k (=1.0) and σ_ε (=1.3) are the turbulent Prandtl numbers for k and ε , respectively.

The pressure-velocity coupling used was SIMPLE, with final second order spatial discretization methods for pressure, momentum, turbulent kinetic energy (k), and turbulent dissipation rate (ε). The convergence criteria were set to 1×10^{-6} for all the residuals.

The simulation was initialized with the first order spatial discretization parameters and default under-relaxation factors ($URFs$) until the residuals' stabilization. Once the residual stability was achieved, the spatial discretization parameters were changed to second order upwind and the $URFs$ to 0.15 for pressure and 0.4 for density, body forces, momentum, turbulent kinetic energy (k), turbulent dissipation rate (ε) and turbulent viscosity (μ_t).

3. Results and Discussions

The simulation results are presented as a function of geometry and position of the buildings, distinguishing cases with the same height, low and high-rise building cases (at side, corner windward, and corner leeward).

Due to the different shapes and sizes of the buildings, there was a variation in the magnitudes of the different parameters under consideration. There was also a change in flow direction at various points due to buildings, which caused a change in magnitude. The variations in the parameters' magnitudes help in understanding the feasibility of airflow and natural ventilation around buildings and street canyons. As specified in Section 2.1, the height of each floor of the building was 4 m. The reference plane for the analysis was set at 1.5 m above the ground of each floor. The airflow velocities and the corresponding static pressures at different locations in the reference planes can be viewed in the contour plots.

3.1 Contour Plot Presentation of the Cases

Fig. 6 shows the static pressure contour developed around the buildings due to airflow. The change in pressure gradient can be noticed from the first buildings (left in the figure) to the last buildings (right in the figure). As the first buildings are directly facing the incoming airflow, there is a maximum pressure on the walls facing the airflow and then it gradually decreases.

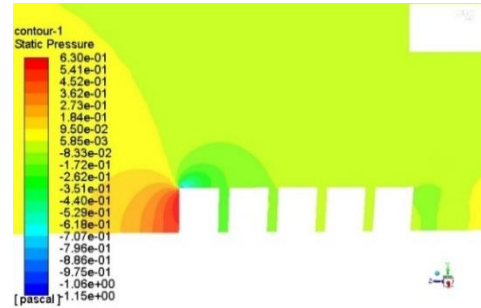


Fig. 6 – Static pressure contour for buildings with same height

Fig. 7 presents the contour plot of velocity around the reference plane on the side. The street aspect ratio (AR_{street}) for the case of buildings with the same height is 1.2 and the aspect ratio ($AR_{building\ gap}$), considering the gap between the buildings, is 4.8, which greatly affects the airflow behavior and natural ventilation around the buildings.

$$AR_{street} = \frac{H_{target\ building}}{Street\ width} \tag{7}$$

$$AR_{building\ gap} = \frac{H_{target\ building}}{Gap\ between\ buildings} \tag{8}$$

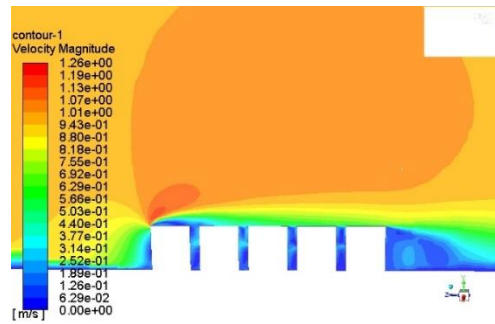


Fig. 7 – Velocity contour for buildings with same height

As mentioned in the literature, there are three main flow regimes: isolated roughness flow regime (IRF , $AR < 0.1-0.125$), wake interference flow regime (WIF , $0.1 < AR < 0.67$) and skimming flow regime with one main vortex (SF , $0.67 < AR < 1.67$) (Yang, et al., 2020).

However, in the configuration with buildings with same height, the $AR_{building\ gap}$ is 4.8, i.e., much higher than the skimming flow regime case. Indeed, two vortices with low intensity can be observed in the gaps between the buildings (Figure 8).

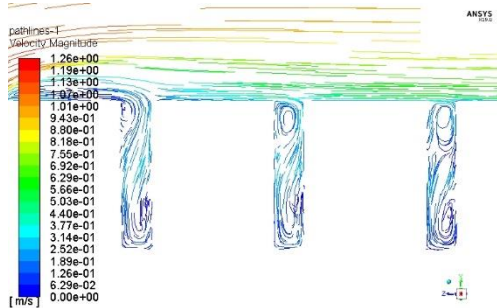


Fig. 8 – Velocity path lines for buildings with same height (side view)

The cases of high-rise and low-rise buildings represent the step-up and step-down canyon cases (Li et al., 2020; Park et al., 2020). The $AR_{building\ gap}$ for high-rise and low-rise buildings is 7.2 and 2.4, respectively. Depending on the location of the high-rise and low-rise buildings, step-up and step-down canyons were decided.

The pressure contours for different cases of high-rise and low-rise buildings indicate that there is a similar trend in the pressure distribution for different buildings configurations, as mentioned at the beginning of this section. This can be seen from Figures 9 to 14 for the high-rise building cases.

Figs. 15 to 20 represent velocity contour plots for low and high-rise building cases. Great variation in the velocity magnitude can be seen near building walls and around buildings, as illustrated by the velocity contour plots illustrate. In addition, as previously mentioned, there is an occurrence of vortices in the gap between buildings which assist airflow around buildings. Flow has been diverted due to buildings being obstacles and there is a recirculation of the airflow at the top of the buildings. This also an essential condition to have an airflow around buildings and, in turn, suitable for natural ventilation around and inside the buildings.

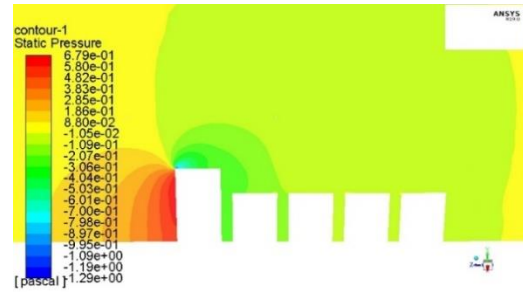


Fig. 9 – Pressure contour plot for high-rise building at windward position



Fig. 10 – Pressure contour plot for high-rise building at center-side position

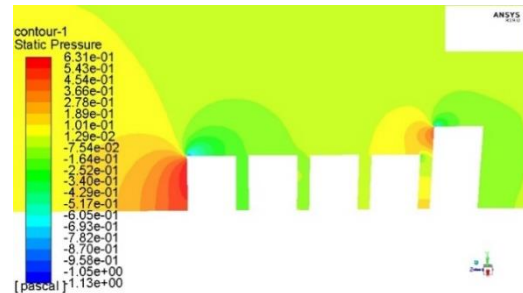


Fig. 11 – Pressure contour plot for high-rise building at leeward position



Fig. 12 – Pressure contour plot for low-rise building at windward position

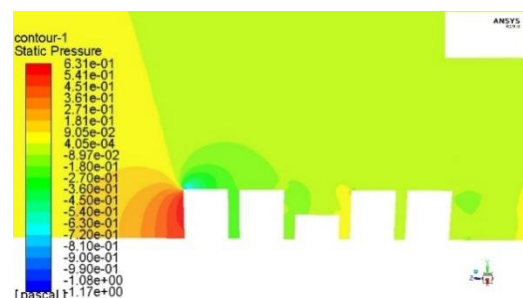


Fig. 13 – Pressure contour plot for low-rise building at center-side position

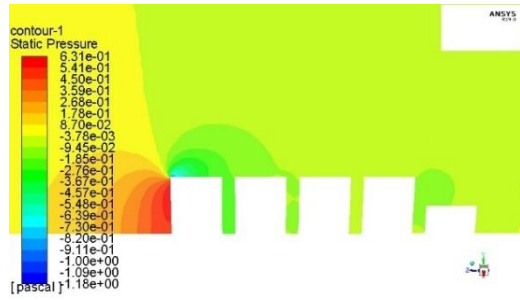


Fig. 14 – Pressure contour plot for low-rise building at leeward position

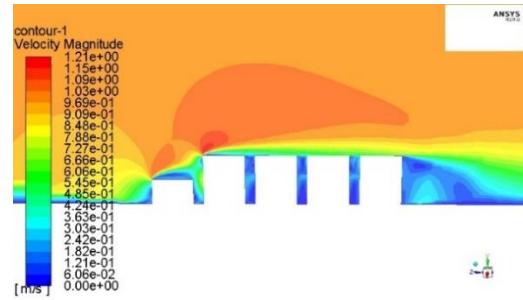


Fig. 18 – Velocity contour plot for low-rise building at windward position

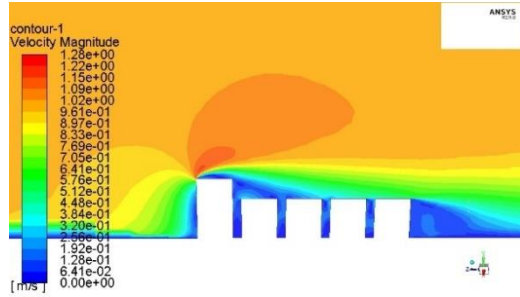


Fig. 15 – Velocity contour plot for high-rise building at windward position

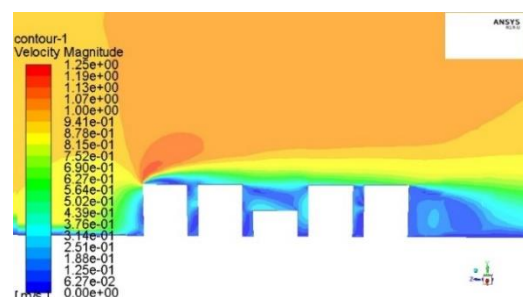


Fig. 19 – Velocity contour plot for low-rise building at center-side position

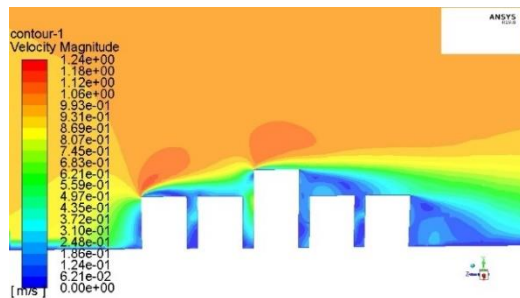


Fig. 16 – Velocity contour plot for high-rise building at center-side position

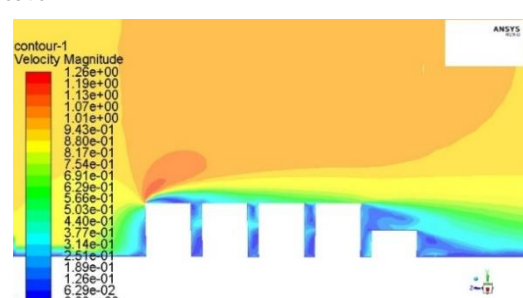


Fig. 20 – Velocity contour plot for low-rise building at leeward position

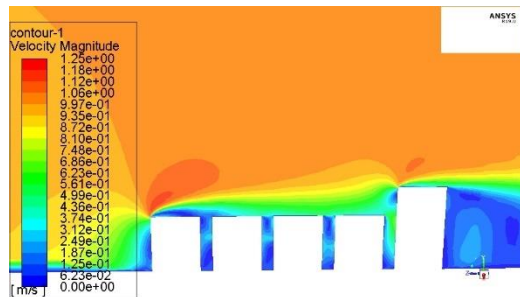


Fig. 17 – Velocity contour plot for high-rise building at leeward position

3.2 Graphical Representation of the Cases

The graphs in Figs. 21 to 24 illustrate the velocity and pressure plots determined at different heights at a distance of 1 m from the walls of the building facing the street. The vertical distance represented in the graphs is a normalized vertical distance, calculated as the ratio of the vertical distance of the point measured from the ground ($Y_{position}$) to the height of the target building (H). Similar criteria are set for the normalized velocity, which is the ratio of the velocity at the corresponding point (V_{mag}) to the reference velocity (V_{ref}) of 1 m/s.

It can be observed from Figs. 21 and 22 that the graphs for the high-rise buildings ($AR_{street,high-rise,1} = 1.8$, $AR_{street,high-rise,2} = 1.2$) in the center and leeward positions have a similar trend, while that is not true in case of the building in the windward position,

characterized by higher airflow velocities and pressures. This suggests higher potential of exploitation of natural solutions for the ventilation of the indoor environments of that building.

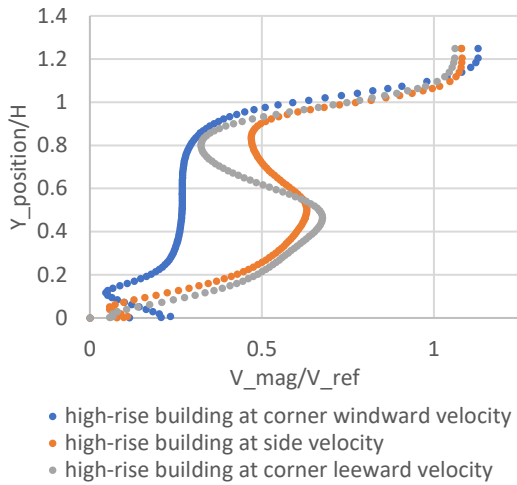


Fig. 21 – Velocity plot for high-rise buildings (1m from the wall facing the street)

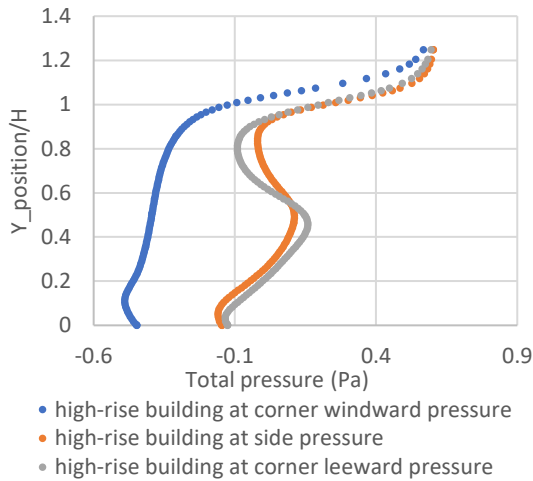


Fig. 22 – Total pressure plot for high-rise buildings (1m from the wall facing the street)

In the case of low-rise buildings ($AR_{street,low-rise,1} = 0.6$, $AR_{street,low-rise,2} = 1.2$) (Fig. 23 and 24), similar trends can be observed, with an increase in velocity and pressure magnitudes along the vertical distance of the target building. Low-rise windward buildings do not follow the same path as the other two low-rise building cases.

In the windward cases of both high- and low-rise buildings, the first buildings experience the decrease in velocity and pressure at ground floor level. This occurs because these buildings are directly facing the wind flow, which causes air recirculation (as it can be noticed from Figs. 15 to 20), resulting in the decreased velocity and pressure.

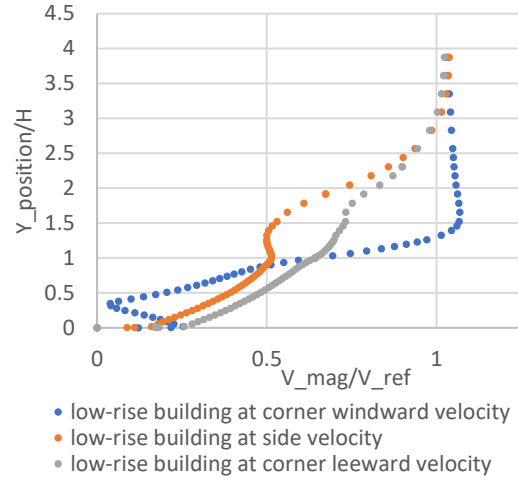


Fig. 23 – Velocity plot for low-rise buildings (1m from the wall facing the street)

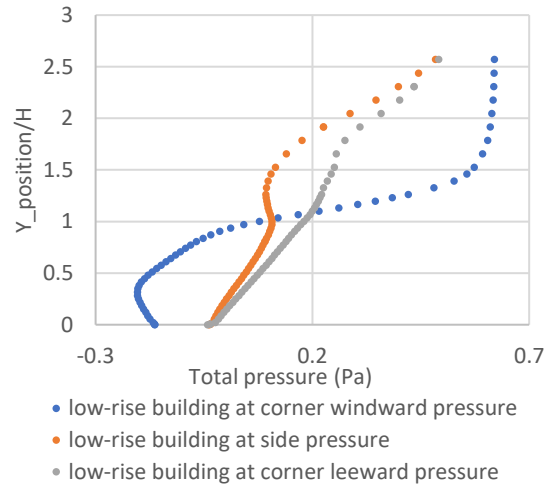


Fig. 24 – Total pressure plot for low-rise buildings (1m from the wall facing the street)

4. Conclusion

This work is a preliminary parametric CFD study about the behavior of airflow around the buildings in different configurations. The analysis focused on the generic building layout of street canyons, considering same-height buildings and different types of target building (high-rise, low-rise). Seven configurations were evaluated, each time focusing on the air displacement around a target building, located respectively at the beginning, at the end, or in the middle of the street canyon, and a case of same height building layout. Pressure and velocity variations were analyzed at different floors of the building façade, also with the help of CFD contour plots.

We observed that, considering the higher aspect ratio of the gaps between buildings in comparison with that of the street canyon, vortices can be easily generated, inducing a recirculation that could facilitate the exploitation of natural ventilation solutions at the different floors of the target building. From the contour and graphic results, it can also be stated that specific building configurations and building positions (e.g., high-rise and low-rise building at the center and the leeward position in the street canyon) show higher potential for exploiting natural solutions for the ventilation of the indoor environments. On the contrary, the buildings in a windward position show a poorer performance.

Further developments of this preliminary research will address validation and generalization of the findings. First, the obtained results will be verified and validated against small-scale experimental tests. Then, multiple configurations of street canyons will be simulated, with the goal of developing a set of rules and simplified correlations useful to engineers, architects, and urban planners to discuss natural ventilation potential from the early stages of new building design or retrofitting of the existing ones.

References

- Chatzimichailidis, A. E., C. D. Argyropoulos, M. J. Assael, and K. E. Kakosimos. 2019. "Implicit Definition of Flow Patterns in Street Canyons—Recirculation Zone—Using Exploratory Quantitative and Qualitative Methods." *Atmosphere* 10(12): 794. doi: <https://doi.org/10.3390/atmos10120794>
- Cheng, W. C., C.-H. Liu, and D. Y. C. Leung. 2009. "On the comparison of the ventilation performance of street canyons of different aspect ratios and Richardson number." *Building Simulation* 2 (1): 53-61. doi: <https://doi.org/10.1007/S12273-008-8332-4>
- CTI. 2016. Comitato Termotecnico Italiano Energia e Ambiente. www.cti2000.it
- Ding, C., and K. P. Lam. 2019. "Data-driven model for cross ventilation potential in high-density cities based on coupled CFD simulation and machine learning." *Building and Environment* 165: 106394. doi: <https://doi.org/10.1016/j.buildenv.2019.106394>
- Guo, F., Y. Fan, and H. Zhang. 2015. "Natural Ventilation Performance in a High Density Urban Area Based on CFD Numerical Simulations in Dalian." In *Proceedings of ICUC9 - 9th International Conference on Urban Climate jointly with 12th Symposium on the Urban Environment*.
- King, M.-F., H. L. Gough, C. Halios, J. F. Barlow, A. Robertson, R. Hoxey, and C. J. Noakes. 2017. "Investigating the influence of neighbouring structures on natural ventilation potential of a full-scale cubical building using time-dependent CFD." *Journal of Wind Engineering and Industrial Aerodynamics* 169: 265-279. doi: <https://doi.org/10.1016/j.jweia.2017.07.020>
- Li, Z., T. Shi, Y. Wu, H. Zhang, Y.-H. Juan, T. Ming, and N. Zhou. 2020. "Effect of traffic tidal flow on pollutant dispersion in various street canyons and corresponding mitigation strategies." *Energy and Built Environment* 1(3): 242-253. doi: <https://doi.org/10.1016/j.enbenv.2020.02.002>
- Padilla-Marcos, M. Á., A. Meiss, and J. Feijó-Muñoz. 2017. "Proposal for a simplified CFD procedure for obtaining patterns of the age of air in outdoor spaces for the natural ventilation of buildings." *Energies* 10(9): 1252. doi: <https://doi.org/10.3390/en10091252>
- Park, S.-J., J.-J. Kim, W. Choi, E.-R. Kim, C.-K. Song, and E. R. Pardyjak. 2020. "Flow Characteristics Around Step Up Street Canyons with Various Building Aspect Ratios." *Boundary-Layer Meteorology* 174(3): 411-431. doi: <https://doi.org/10.1007/s10546-019-00494-9>
- Peng, Y., X. Ma, F. Zhao, C. Liu, and S. Mei. 2017. "Wind driven natural ventilation and pollutant dispersion in the dense street canyons: Wind Opening Percentage and its effects." *Procedia Engineering* 205: 415-422. doi: <https://doi.org/10.1016/j.proeng.2017.10.392>
- Peng, Y., Z. Gao, R. Buccolieri, and W. Ding. 2019. "An Investigation of the Quantitative Correlation between Urban Morphology Parameters and Outdoor Ventilation Efficiency Indices." *Atmosphere* 10(1): 33. doi: <https://doi.org/10.3390/atmos10010033>
- Ramponi, R., B. Blocken, L. B. de Coo, and W. D. Janssen. 2015. "CFD simulation of outdoor

- ventilation of generic urban configurations with different urban densities and equal and unequal street widths." *Building and Environment* 92: 152-166. doi: <https://doi.org/10.1016/j.buildenv.2015.04.018>
- Song, J., S. Fan, W. Lin, L. Mottet, H. Woodward, Davies M. Wykes, R. Arcucci, et al. 2018. "Natural ventilation in cities: the implications of fluid mechanics." *Building Research and Information* 46(8): 809-828. doi: <https://doi.org/10.1080/09613218.2018.1468158>
- United Nations. 2018. "The World's Cities in 2018." https://www.un.org/en/events/citiesday/assets/pdf/the_worlds_cities_in_2018_data_booklet.pdf
- Yang, X., Y. Zhang, J. Hang, Y. Lin, M. Mattsson, M. Sandberg, M. Zhang, and K. Wang. 2020. "Integrated assessment of indoor and outdoor ventilation in street canyons with naturally-ventilated buildings by various ventilation indexes." *Building and Environment* 169: 106528. doi: <https://doi.org/10.1016/j.buildenv.2019.106528>
- Yuan, C., and E. Ng. 2012. "Building porosity for better urban ventilation in high-density cities - A computational parametric study." *Building and Environment* 50: 176-189. doi: <https://doi.org/10.1016/j.buildenv.2011.10.023>